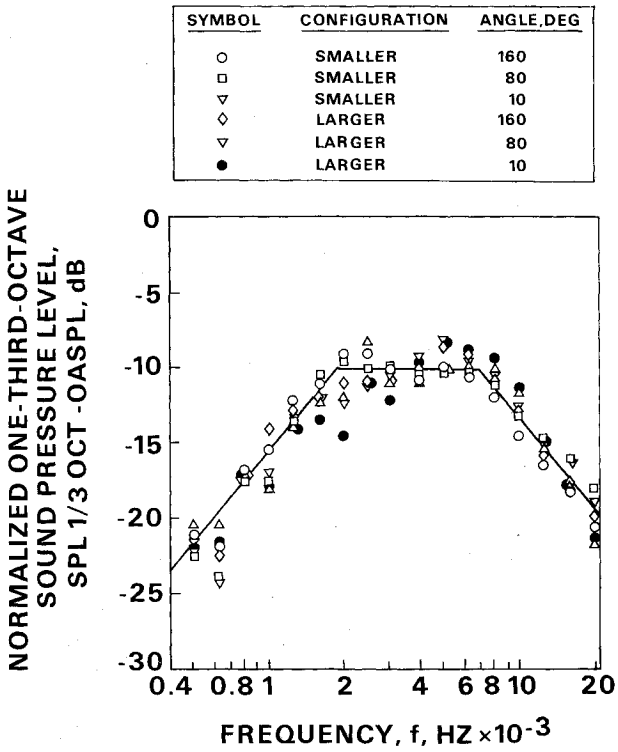

Fig. 3 Normalized spectra for semicylinder reversers.

References

[1]Gutierrez, O. A. and Stone, J. R., "Preliminary Experiments on the Noise Generated by Target-Type Thrust Reverser Models," TM X-2553, May 1972, NASA.

[2]Stone, J. R. and Gutierrez, O. A., "Target-Type Thrust Reverser Noise," *Journal of Aircraft*, Vol. 10, No. 5, May 1973, pp. 283–288; also TM X-68082, Aug. 1972, NASA.

[3]Ffowcs Williams, J. and Hall, L. H., "Aerodynamic Sound Generation of Turbulent Flow in the Vicinity of a Scattering Half Plane," *Journal of Fluid Mechanics*, Vol. 40, Pt. 4, March 1970, pp. 657–670.

Unique Characteristics of Exhaust-Plume Interference

Dave Bergman*

Convair Aerospace Division of General Dynamics Corporation/Fort Worth Operation, Fort Worth, Texas

Nomenclature

A = cross-sectional area
C_D = drag coefficient, $D/(q_0 A_m)$
C_{Dp} = pressure drag coefficient, $(1/A_m)\int_{Am}^{Ab} C_p dA$
C_p = pressure coefficient, $(p - p_0)/q_0$
D = nozzle external drag
M = Mach number
NPR = nozzle pressure ratio, P_j/p_0
P_j = nozzle-exhaust total pressure
p = static pressure
q = dynamic pressure

Subscripts

b = nozzle end
m = nozzle maximum
o = freestream

Received December 6, 1972; revision received June 13, 1973.

Index categories: Jets, Wakes, and Viscid-Inviscid Flow Interactions; Subsonic and Supersonic Airbreathing Propulsion; Aircraft Powerplant Design and Installation.

*Senior Propulsion Engineer, Aerospace Technology Department. Member AIAA.

Introduction

AERODYNAMIC interference is a term often used to describe the interactions between closely spaced solid bodies. But interference between solid bodies and plumes also occurs. For example, jet-engine exhaust plumes can significantly affect aerodynamic forces on nearby airplane structure. In fact, this frequently happens. Studies have shown that airplane drag, lift, and moments can vary if plume conditions change.[1-8]

What complicates the prediction of plume interference is that plumes, unlike solid bodies, create entrainment effects as a result of viscous shear, or mixing, with the surrounding flow. Yet plumes are also obstacles to the surrounding flow, as are solid bodies. Therefore, plume interference can be depicted as being a composite of two constituents, plume entrainment and plume shape, which iteracts with airplane flowfields.

Objectives and Methodology

Researchers using various techniques have examined the fundamental case of jet interference on isolated exhaust nozzles.[9-12] Changes in plume conditions, such as different pressure ratios, can significantly change nozzle external drag. These interference effects are more noticeable during subsonic and transonic flight than during supersonic flight. At supersonic speeds, disturbances can transmit upstream, toward the nozzle, only through the relatively small subsonic portion of the nozzle boundary layer.

Exhaust plumes are represented in some analyses as being solid bodies, often cylinders.[13-16] This is obviously a simplification of the true situation; nevertheless, it is an approach sometimes used for pragmatic reasons. So that such approaches may be evaluated, an objective of this study was to compare, experimentally, flowing jets with

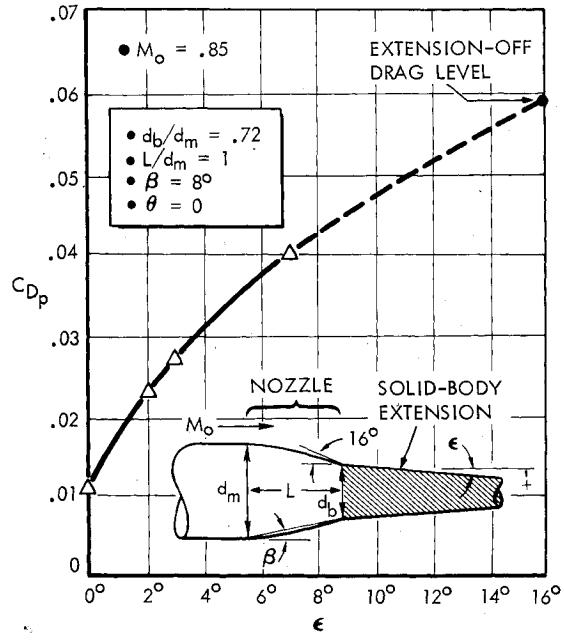

Fig. 1 Effects of solid-body plume simulators on nozzle pressure drag.

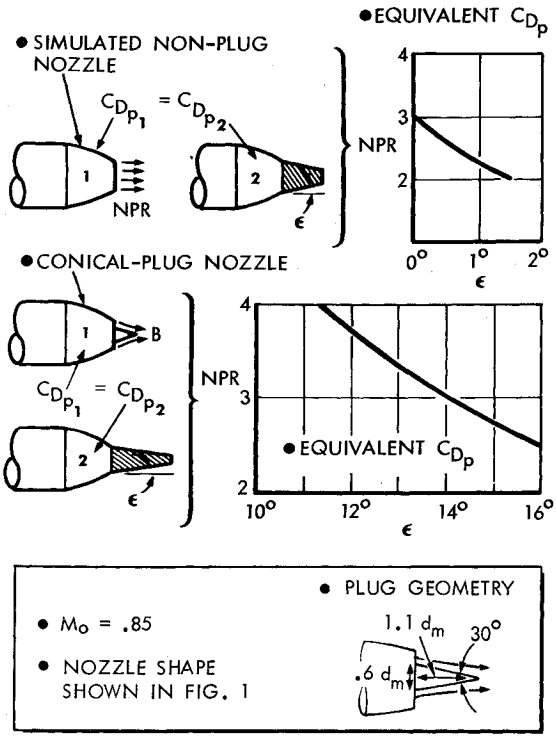

Fig. 2 Equivalent drag crossplots.

solid-body plume simulation. Another objective was to examine plume interference effects associated with changes in nozzle shape as well as changes in plume condition.

Experiments were conducted in a freejet wind-tunnel facility at the Fort Worth operation of the Convair Aerospace Division. Descriptions of this facility have been published.[17] All the nozzle models tested are bodies of revolution, 3 in. in maximum external diameter. These models have circular-arc external contours and their internal flow areas become minimal at their exit plane. Each nozzle, connected to a cylindrical upstream-support pipe, is subjected to changes in freestream Mach number and nozzle pressure ratio (exhaust total pressure divided by freestream static pressure). External surface flow at the nozzle connect station has a turbulent boundary layer, its height being approximately 17% of the pipe diameter. Rows of static-pressure orifices comprise the model external instrumentation. The pressure readings from these orifices are plotted vs aft-facing projected area and then integrated to obtain nozzle pressure drag. In addition, total-pressure tubes located inside each nozzle measure nozzle pressure ratio. All instrumentation is of the steady-state type, connected to a scanivalved transducer located outside the test section.

Results and Analysis

Solid-body plume simulation

Several solid-body extensions, or "plume simulators," were alternately attached to a nozzle, as shown in the insert sketch on Fig. 1. For simplicity, these extensions were conical shapes, with the half angle of each denoted as ϵ. Nozzle pressure drag, plotted in Fig. 1, increases several fold as the extensions proceed from being cylindrical ϵ = 0, through the conics tested, up to ϵ = 7°. The nozzle drag increases because, as the solid extensions become more tapered, less flow recompression occurs near the end of the nozzle. For example, nozzle drag at ϵ = 1.5° is twice that at ϵ = 0. Thus, seemingly small changes in extension shape can cause large changes in the upstream flowfield. The dashed line extending from ϵ = 7° to 16° in Fig. 1 is an extrapolation to the drag level that occurs with no extension attached and with no exhaust flow. Note that the end of the nozzle is at a 16° angle; thus extrapolating

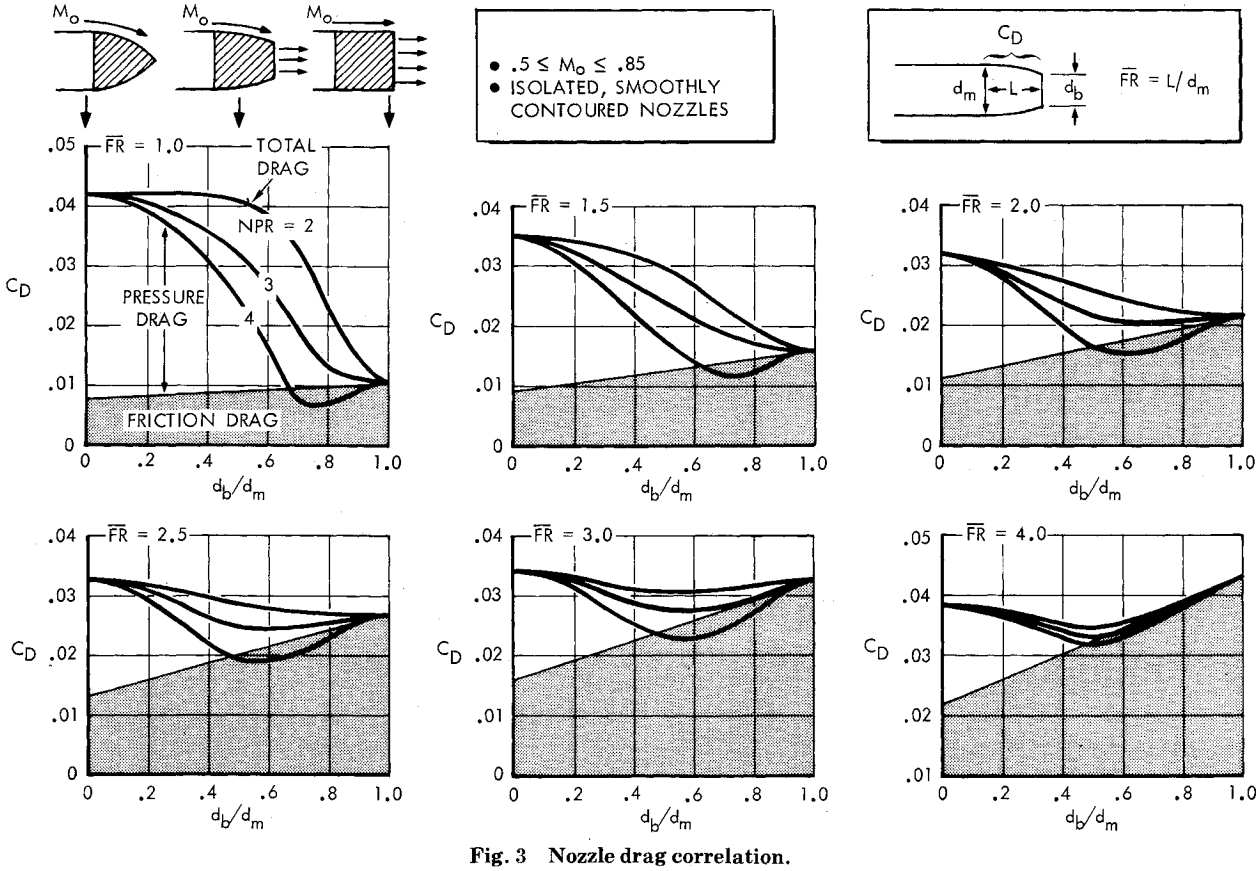

Fig. 3 Nozzle drag correlation.

to an ϵ corresponding to this value for the jetoff condition seems within reason, at least for the sake of example.

Next, the solid extensions were replaced with flowing jets. Two types of plumes were tested: one representing a nonplug-nozzle exhaust plume, the other an exhaust plume surrounding a conical centerbody plug. Again, nozzle pressure drag was measured. But, rather than varying ϵ, data were taken at several nozzle pressure ratios from jet off to 4. Forces occurring on the centerbody plug itself were not measured in these experiments.

The jeton and the solid-extension results were combined to produce the crossplots shown in Fig. 2. The purpose here is to ascertain what solid-extension shapes produce nozzle drag levels equivalent to those at jeton conditions. For the nonplug nozzle, one might expect the plume shape to be cylindrical at ideally expanded, just-choked conditions ($NPR \approx 2$); however, it is especially significant in Fig. 2 that at this NPR a solid body narrower than a cylinder is required to simulate jet interference; the "effective" plume shape is cylindrical only when the plume billows at the underexpanded $NPR = 3$ condition. A conic solid body having a 1.5° half angle produces the correct interference effects at $NPR = 2$ for the nonplug nozzle, but note that at NPR's from 2 to 2.5, no solid body can simulate the same interference on the plug-type nozzle; in other words the plug nozzle tested has more external drag (excluding plug forces) at NPR's from 2 to 2.5 than at jetoff conditions. Apparently, plume entrainment, a unique characteristic of exhaust-plume interference, plays an important role in producing these interference effects.

The solid-body shapes required to generate equivalent plume-interference effects on the plug nozzle at NPR's greater than 2.5 are more tapered than those appropriate for the nonplug nozzle. This is an expected result because the plume attempts to follow the tapered centerbody-plug contour.

To retain proper perspective, it should be emphasized that these results are linked to specific nozzles and cannot be expected to be independent, at least quantitatively, of aftbody/nozzle geometry.

Nozzle drag correlation

Nozzle drag correlations are desirable for establishing general overviews of nozzle behavior as engine power setting and nozzle geometry vary. Drag data from this study plus other recent Convair studies[17-19] were compiled along with other empirical data[9,13,20,21] to generate the curves presented in Fig. 3. The two geometric parameters used here are nozzle fineness ratio (nozzle length divided by nozzle maximum diameter) and diameter ratio (d_b/d_m). Only smoothly contoured nozzle shapes, e.g., circular arc or parabolic, having thin trailing edges are considered here; nozzles having abrupt contour changes and/or thick bases usually exhibit a different drag behavior.

Total nozzle drag and its components, pressure drag and friction drag, are shown in the plots of Fig. 3. Notice that the nozzle shape at $d_b/d_m = 0$ reaches an imaginary boundary condition where no exhaust orifice exists; here the pressure drag is large compared to the friction drag. The opposite occurs at $d_b/d_m = 1$, where the larger surface area causes friction drag to increase considerably, but the cylindrical shape prevents pressure drag from occurring.

Increases in fineness ratio result in decreased pressure drag but increased friction drag. In the limit, pressure drag approaches zero as fineness ratio approaches infinity; however, in practical terms, pressure drag for a typical range of nozzle positions ($0.4 < d_b/d_m < 1$) rapidly approaches a negligible level when a fineness ratio of 4 is reached. Changes in exhaust area and/or nozzle pressure ratio noticeably affect total drag at fineness ratios less than 4; at 4, plume-interference effects are not large since the exhaust plume is somewhat remote with respect to the overall nozzle surface. Fineness ratios from 1.5 to 2 apparently produce the least amount of pressure-plus-friction drag.

Increases in nozzle pressure ratio from an $NPR = 2$ to 3 or 4 result in less nozzle drag at fineness ratios between 1 and 4. However, nozzle thrust efficiency is reduced for convergent nozzles at underexpanded-plume conditions. Nozzle selection criteria must therefore involve thrust-minus-drag tradeoffs to account for these effects.

Conclusions

Exhaust-plume interference on nozzle drag is a function of plume entrainment as well as plume shape. In some situations, certain solid bodies—with narrower shapes than might be expected—can be used in place of plumes to simulate plume interference on drag. However, there are also some nozzle geometry and pressure-ratio conditions in which solid bodies cannot simulate exhaust-plume interference. Therefore, one must carefully examine situations involving solid-body plume simulation.

The drag of isolated, smoothly contoured nozzles with typical exhaust conditions is significantly affected by plume interference at nozzle length-to-diameter ratios below 4. Of the nozzle configurations considered, length-to-diameter ratios from 1.5 to 2 produce the least amount of pressure-plus-friction drag.

References

[1]Carter, A. W., "Effects of Jet-Exhaust Location on the Longitudinal Aerodynamic Characteristics of a Jet V/STOL Model," TN D-5333, July 1969, NASA.

[2]Patterson, J. C., Jr. and Flechner, S. G., "Jet Wake Effect of a High-Bypass Engine on Wing-Nacelle Interference Drag of a Subsonic Transport Airplane," TN D-6067, Nov. 1970, NASA.

[3]August, H., "B-1 Airplane Model Support and Jet Plume Effects on Aerodynamic Characteristics," AIAA Paper 73-153, Washington, D.C., 1973.

[4]Glasgow, E. R. and Santman, D. M., "Aft-End Design Criteria and Performance Prediction Methods Applicable to Air Superiority Fighters Having Twin Buried Engines and Dual Nozzles," AIAA Paper 72-1111, New Orleans, La., 1972.

[5]Miller, E. H. and Migdal, D., "Subsonic Interference Characteristics of Single and Twin Jet Afterbodies," *Journal of Aircraft*, Vol. 7, No. 3, May–June 1970, pp. 261–266.

[6]Schnell, W. C. and Migdal, D., "An Experimental Evaluation of Exhaust Nozzle/Airframe Interference," *Journal of Aircraft*, Vol. 7, No. 5, Sept.–Oct. 1970, pp. 395–400.

[7]Throndson, L. W., "Close-Spaced Nozzles Twin Jet Configuration," AIAA Paper 70-934, Los Angeles, Calif., 1970.

[8]Motycka, D. L. and Skowronek, P. J., Jr., "Performance Installation Effects for Nozzles Installed on a Twin-Jet Fighter Airplane Model," SAE Paper 680296, New York, 1968.

[9]Harrington, D. E., "Performance of Convergent and Plug Nozzles at Mach Numbers from 0 to 1.97," TM X-2112, Oct. 1970, NASA.

[10]Glasgow, E. R., Divita, J. S., Everling, P. C., and Laughrey, J. A., "Analytical and Experimental Evaluation of Performance Prediction Methods Applicable to Exhaust Nozzles," AIAA Paper 71-719, Salt Lake City, Utah, 1971.

[11]Englert, G. W., Vargo, D. J., and Cubbison, R. W., "Effect of Jet-Nozzle-Expansion Ratio on Drag of Parabolic Afterbodies," RM E54B12, April 1954, NASA.

[12]Harrington, D. E., "Jet Effects on Boattail Pressure Drag of Isolated Ejector Nozzles at Mach Numbers From 0.60 to 1.47," TM X-1785, May 1969, NASA.

[13]Shrewsbury, G. D., "Effect of Boattail Juncture Shape on Pressure Drag Coefficients of Isolated Afterbodies," TM X-1517, March 1969, NASA.

[14]Grund, E., Presz, W., Jr., and Konarski, M., "Predicting Airframe/Exhaust Nozzle Interactions at Transonic Mach Numbers," AIAA Paper 71-720, Salt Lake City, Utah, 1971.

[15]Blaha, B. J., "Effect of Underwing Engine Nacelle Shape and

Location on Boattail Drag and Wing Pressures at Mach Numbers From 0.56 to 1.46," TM X-1979, March 1970, NASA.

[16]Presz, W., Jr., Konarski, M., and Grund, E., "Prediction of Installed Nozzle Flowfields," *Journal of Aircraft*, Vol. 8, No. 12, Dec. 1971, pp. 988–994.

[17]Bergman, D., "Effects of Engine Exhaust Flow on Boattail Drag," *Journal of Aircraft*, Vol. 8, No. 6, June 1971, pp. 434–439.

[18]Bergman, D., "Exhaust Nozzle Drag: Engine vs Airplane Force Model," *Journal of Aircraft*, Vol. 8, No. 10, Oct. 1971, pp. 825–830.

[19]Bergman, D., "An Aerodynamic Drag Study of Jet Engine Nozzles," AGARD Paper 22, CP-91-71, Sept. 1971.

[20]Henry, B. Z., Jr. and Cahn, M. S., "Additional Results of an Investigation at Transonic Speeds to Determine the Effects of a Heated Propulsion Jet on the Drag Characteristics of a Series of Related Afterbodies," RM L56G12, Sept. 1956, NACA.

[21]Rustemeyer, A. H. and Twomey, E. J., "Thrust and Drag Characteristics of Several Turbojet Exhaust Models at Supersonic and High-Subsonic Mach Numbers," R-0922-16, June 1957, United Aircraft Corp., Hartford, Conn.

Angular Momentum and the Aircraft-Store Separation Problem

P. Daniels* and T. A. Clare*
Naval Weapons Laboratory, Dalgren, Va.

Nomenclature

F_{xA},F_{yA},F_{zA}	= forces along the X_A, Y_A, Z_A axes
F_{xB},F_{yB},F_{zB}	= forces along the X_B, Y_B, Z_B axes
I_x,I_y	= rolling and pitching moments of inertia
I_{x_2},I_{y_2}	= rolling moment of intertia of outer body and inner body
I_{y1},I_{y_2}	= pitching moment of inertia of outer body and inner body
K_1,K_2	= complex constants defined by the initial conditions
m	= total configuration mass
m_1,m_2	= masses of outer and inner bodies
$M_{p\dot{\alpha}}$	= Magnus moment stability derivative
$M_q + M_{\dot{\alpha}}$	= pitch damping moment stability derivative
M_{xA},M_{yA},M_{zA}	= moments about the X_A, Y_A, Z_A axes
M_{xB},M_{yB},M_{zB}	= moments about the X_B, Y_B, Z_B axes
M_α	= pitching moment stability derivative
p,q,r	= angular velocity components resolved along the X, Y, Z axes
s	= gyroscopic stability factor
t	= time
$\dot{u},\dot{v},\dot{w}$	= body linear velocity components resolved along X, Y, Z axes
X,Y,Z	= right handed coordinate system when X is the missile axis of symmetry
x_1	= distance from c.g. of outer body to total configuration c.g.
x_2	= distance from c.g. of inner body to total configuration c.g.
Z_α	= normal force stability derivative
α	= Complex angle of attack
$\lambda_{1,2}$	= dynamic damping factors
ω_1,ω_2	= nutation and precession frequencies

Subscripts

A	= aeroballistic axis system
B	= body fixed axis system
1	= outer body
2	= inner body

Received May 10, 1973; revision received May 30, 1973. Acknowledgement is due to C. J. Cohen, Research Associate for the Warfare Analysis Department. Equation (2) is due to him.

Index category: LV/M Dynamics, Uncontrolled.

*Research Scientist, Warfare Analysis Department. Member AIAA.

Introduction

AIRCRAFT-store separation is a serious consideration for both weapon and aircraft designers. The weapon designer wants to avoid the large release disturbance since it affects the weapons accuracy. The aircraft designer wants to avoid the large release disturbance since it is dangerous to the pilot and can result in damage to the aircraft.

There have been various methods of improving weapon separation characteristics but none has been entirely satisfactory since they are based largely upon trial and error. Present systems are rather erratic in their separation characteristics due to variation in store configurations.

In retrospect, it is quite unlikely that a store separation problem existed when aircraft flew at 250 knots and dropped 2000 lb bombs due to the inertia loads being much greater than the aerodynamic loads. The bombs were aerodynamically inert at release.

However, aircraft speed has increased considerably. The aerodynamic loads increased with velocity squared and store separation became a problem. Weapon accuracy was reduced and aircraft damage was sustained.

Aircraft can now carry high density, externally stored weapons supersonically. It would also be advantageous to launch these weapons supersonically. The aerodynamic loads will be much larger and if large release disturbances are encountered, the damage to the aircraft can be severe.

One method of alleviating the store separation is to gyroscopically increase the weapon's inertial forces by inserting a spinning fly wheel. Admittedly, this is an added complication but it may be required to solve the problem. It is the purpose of this paper to present the mechanics of the internally stabilized weapon.

Rigid Body Dynamics

From the linear theory of missile dynamics it can be shown that an approximate solution for the angle of attack of a spinning, symmetric, rigid body (neglecting damping) is

$$\alpha = K_1 e^{(i\omega_1 t)} + K_2 e^{(i\omega_2 t)} \tag{1}$$

If $\alpha_0 = 0$ at $t = 0$ then it may be shown that for an initial angular rate the maximum angle of attack is

$$|\alpha_{MAX}| = 2|\dot{\alpha}_0|/[(p^2 I_x^2/I_y^2) - 4M_\alpha/I_y]^{1/2} \tag{2}$$

Consequently, for statically stable configurations, the maximum angle of attack due to an angular rate may be reduced by increasing the angular momentum or by increasing the restoring moment. It is suggested that external stores be designed in accordance with Eq. (2).

The restoring moment for an external store is usually small due to the design conforming to space limitations. However its angular momentum may be increased considerably.

Two methods of increasing the angular momentum of external stores are readily apparent. The first would require spinning the store on the rack. This method would necessitate a complicated rack design which would probably not work for all stores. Moreover, the stores would be released with a high spin rate and be subject to Magnus instability.

A second method for increasing the angular momentum of an external store is to spin an internally mounted fly wheel. This method would work equally well for all types